System Performance Simulations of the RatCAP Awake Rat Brain Scanner

Sepideh Shokouhi, *Student Member, IEEE*, Paul Vaska, David J. Schlyer, Sean P. Stoll, Azael Villanueva, Jr., Aarti Kriplani, and Craig L. Woody

***Abstract*—The capability to create high quality images from data acquired by the Rat Conscious Animal PET tomograph (RatCAP) has been evaluated using modified versions of the PET Monte Carlo code Simulation System for Emission Tomography (SimSET). The proposed tomograph consists of lutetium oxyorthosilicate (LSO) crystals arranged in 12 4 × 8 blocks. The effects of the RatCAPs small ring diameter (∼40 mm) and its block detector geometry on image quality for small animal studies have been investigated. Since the field of view will be almost as large as the ring diameter, radial elongation artifacts due to parallax error are expected to degrade the spatial resolution and thus the image quality at the edge of the field of view. In addition to Monte Carlo simulations, some preliminary results of experimentally acquired images in both two-dimensional (2-D) and 3-D modes are presented.**

***Index Terms*—SimSET, small animal imaging.**

I. Introduction

CURRENT small animal positron emission tomography (PET) imaging instruments for rats are limited by the need of anesthesia for motion elimination which can profoundly depress brain function [1]. The RatCAP will eliminate the motion of the animal relative to the imaging device by reducing the diameter of a tomograph to such an extent that it can be directly attached to the rat's skull. The feasibility of the proposed geometry has been previously analyzed [2]. A detailed description of the RatCAP design has also been reported [3].

The small diameter of the tomograph (40 mm) is advantageous as it leads to reduced cost due to a smaller number of detectors and better sensitivity due to the increased solid angle coverage. However, the fact that the field of view nearly fills the detector ring might lead to severe parallax effects resulting in radial elongation artifacts [4].

Analyzes were performed in both two-dimensional (2-D) and 3-D mode. Although operating in 3-D mode would increase the sensitivity, a 2-D acquisition can also be considered a reasonable alternative since the sensitivity is more uniform along the axial direction. Furthermore, since the 3-D data were Fourier rebinned before applying a 2-D filtered backprojection, we would expect to get a better axial resolution in 2-D mode than in 3-D mode. The data were not precorrected for scatter and therefore a reasonable energy resolution is necessary for an efficient threshold setting. Even though the small size of a rat's brain results in fewer scattered events than in a larger object, the fraction of scatter events detected is increased due to the larger solid angle encompassed by the scanner.

This paper presents system performance simulations of this new detector system, along with some preliminary 2- and 3-D (Fourier rebinned [5]) images obtained with two detector blocks on a rotational platform that provide tomographic data.

Manuscript received May 9, 2003; revised March 1, 2005. This work was supported in part by a grant from the DOE Office of Biological and Environmental Research and DOE Contract DE-AC02-98CH10886U.S.

S. Shokouhi, A. Villanueva, Jr., and A. Kriplani are with the State University of New York (SUNY) at Stony Brook, Stony Brook, NY 11790 USA (e-mail: sepideh @bnl.gov; azvilla @bnl.gov; aarti@bnl.gov).

P. Vaska, D. J. Schlyer, S. P. Stoll, and C. L. Woody are with Brookhaven National Laboratory, Upton, NY 11973 USA (e-mail: vaska@bnl.gov; schlyer@bnl; stoll@lbnl.gov; woody@bnl.gov).

Digital Object Identifier 10.1109/TNS.2005.858236

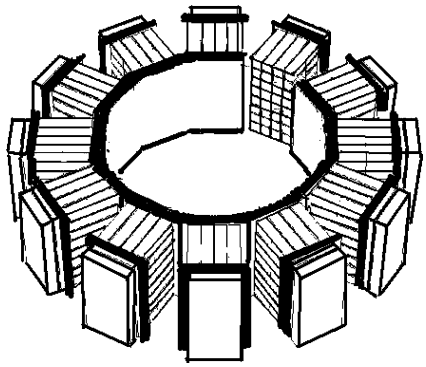

Fig. 1. First prototype of RatCAP consisting of 12 4 × 8 arrays of LSO+APD detector blocks.

II. Materials & Methods

A. Experiments

The first fully operational version of RatCAP (Fig. 1) will consist of 12 LSO-APD (avalanche photodiodes) detector blocks that are arranged in a ring with a diameter of about 40 mm. Each block consists of a 4 × 8 array of LSO-APD elements. In the current stage of our experiment only 2 out of 12 blocks are available. For preliminary image reconstructions, we have placed a rotational platform between the detectors (Fig. 2). Different phantoms (Fig. 3) have been placed on the center of the platform and rotated in desired angular steps. Unfortunately this approach allows for collecting coincident events only between detector blocks which are directly opposite one another whereas in the real RatCAP, nonopposing detectors are also involved in coincident event detection. The fact that we are sampling only from opposite detectors restricts the field of view (FOV) to a circular area with a maximum diameter of 8 mm (the block width) since other lines of response are not available.

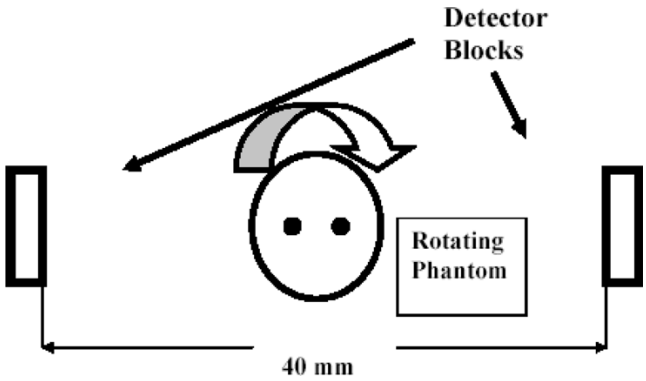

Fig. 2. Phantoms were placed on a rotational platform and rotated in ~13 steps through 180 degrees.

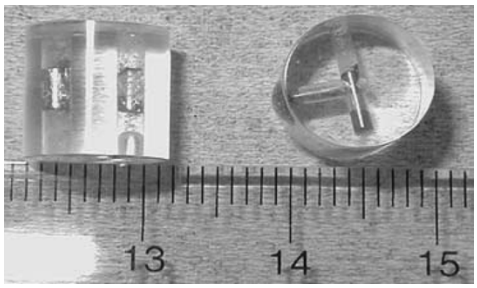

Fig. 3. ^{68}Ge phantoms of two point sources and an L-shaped source.

An advantage of using the phantom rotational platform is the ability to represent a complete ring tomograph without any gaps between the detector blocks. By decreasing the size of the rotational steps we can obtain complete radial and angular sampling. This is useful because, first of all, sinograms with no zero efficiency bins are more compatible with standard filtered back projection reconstruction methods and second, these complete sinograms can be compared with the incomplete sinograms from the operational RatCAP to examine the impact of detector gaps on the image quality.

For the experimental part, two phantoms (2 point sources and an L-shaped source) were placed on a rotational platform between two detector blocks each comprising a 4×8 array of $2 \times 2 \times 10$ mm lutetium oxyorthosilicate (LSO) crystals coupled (via a UV-transparent silicone wafer) to a geometrically matched 4×8 APD array from Hamamatsu (model S8550, with 1.6 mm $\times$ 1.6 mm active area per element). The sources were stainless steel tubes, 1 mm in diameter, filled with resin impregnated with ^{68}Ge. The amounts of activity in the two rods are slightly different. One of the sources contains 9 and the other 11 μCi of ^{68}Ge.

For detecting each coincident event, the APD output signals from all 64 channels (32 from each detector block) were read out and digitized by CAMAC Fast Encoding and Readout Analog to Digital Converters (LeCroy 4300 B). The pulse height spectra from all channels were plotted and fitted to determine the 511-keV photopeak positions. The value of the peak positions together with channel specific pedestal values were used to match the gains among the channels. The gain-corrected pulse height spectra were used to set an energy threshold at 420 keV. The gain-corrected channel with the highest charge output (one channel from each side) was used for event positioning.

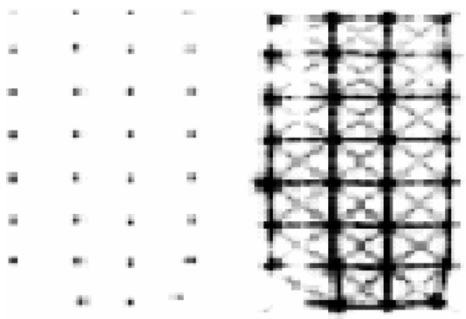

Fig. 4. Flood histogram of a detector block (4×8 array of LSO-APD elements) taken from [9]. The left image is scaled to the pixel with maximum recorded events. The color scale of the right hand image is saturated to show the level of crosstalk between crystals.

A flood histogram of the block detectors is shown in Fig. 4 showing the event positioning and block crystal separation of the detectors.

The coincident events from all rotational positions were binned into sinograms with 7 radial and 13 angular bins. The radial bin size was 1.2 mm, equal to the half of the detector element pitch, encompassing the full 8 mm diameter field of view. The raw angular sampling was chosen to be consistent with a constant detector pitch of 2.4 mm along a circle of radius 20 mm resulting in an equivalent of 52 evenly spaced detectors around the ring rather than the 48 crystals in the RatCAP which are arranged in 12 blocks with gaps between them. This was done to avoid streak artifacts from the gaps. Thus there were a total of 52 different azimuthal angles in this arrangement. Standard interleaving of adjacent angles reduced this by a factor of 2, and furthermore a mash factor of 2 was applied due to the small FOV, resulting in 13 angular bins in the final sinogram. For similar reasons, to achieve the best overlap between adjacent block positions, the platform was rotated in 13 steps of 13.8 degrees each.

A 3-D data acquisition was performed followed by Fourier rebinning (FORE) [5] and filtered back projection. These were compared with the images of 2-D data. The only difference between the 2- and 3-D mode is the type of lines of response (LORs) that were used for sinogram binning. In the 2-D mode, we used only axially direct LORs whereas in the 3-D mode all the LORs (direct and oblique) were used for sinogram binning. The design of our scanner does not include septa. Both 2- and 3-D images were reconstructed using filtered back projection and analysis software supplied with our Concorde microPET R4 system (microPET Manager, version 1.6.4.0). For the 3-D data, various reconstruction protocols were created which incorporated maximum ring differences from 0 to 5. The larger the ring difference, the larger is the copolar coincidence acceptance angle. The maximum possible ring difference for the RatCAP tomograph is 7. As the reconstruction software was written for the Concorde microPET scanners, the 3-D sinograms of RatCAP had to be modified to ensure a correct interpretation of the 3-D sinograms by the reconstruction software. An example is the span value that gives the compression factor of the oblique sinograms in copolar direction. For microPET, which

TABLE I
DATA ACQUISITION PARAMETERS

Data mode	2D	3D	3D	3D
Image planes	8	15	15	15
Maximum ring difference	0	1	3	5
Span	1	1	1	1

has a larger number of axial detector elements (32) relative to RatCAP (8), span values larger than one are reasonable whereas in RatCAP $\mathrm{span} = 1$ (no compression) is required for sufficient sampling.

Unfortunately, $\mathrm{span} = 1$ was not compatible with the image reconstruction software leading to a mis-positioning of the point sources in the axial direction. We have zero-padded the sinograms in order to address this problem. Table I gives a summary of some adjusted parameters in the header file and reconstruction protocol for both 2- and 3-D. The experimental conditions require no arc corrections because only two detectors which were directly opposed were used.

B. Simulations

By using Monte Carlo techniques for PET tomographic applications, positron sources of different sizes and shapes can be simulated and their annihilation photons tracked within the tomograph. We have used simulation system for emission tomography (SimSET) for the RatCAP simulations. The SimSET package has been developed by the Imaging Research Laboratory at the University of Washington [6]. It is written in a modular format. For PET simulations, 3 modules were required. The first module is the photon history generator (PHG) where the generation and transportation of photons within the user-defined object are tracked. This module is followed by the detector module where the detector geometry and material are specified. The last module is the binning module that takes care of the detection records and creates output files. We have used SimSET versions 2.6.2.2 through 2.6.2.4. Since none of these versions provides block detector geometry, we had modified some of its codes to closely simulate block detector geometry by using a cylindrical PET in the detector module and writing a routine to simulate the behavior of a discrete-crystal block-detector tomograph. The original (not modified) cylindrical PET option models a tomograph with a depth of interaction measurement capability because the coincident events are binned based on their exact interaction positions within an LSO crystal annulus.

The discretization process that was implemented can be described as a nearest crystal selection for each of the two gamma-rays in coincidence, based on the input block structure. A valid event is binned into 3-D sinograms in the standard way. The user can define how (and whether) to do discrete crystal-binning in an additional parameter file. Two different discretization methods were developed. The earlier code did not take the gaps between the detector blocks into account. This version was used to estimate the impact of the LSO crystal length on the parallax error.

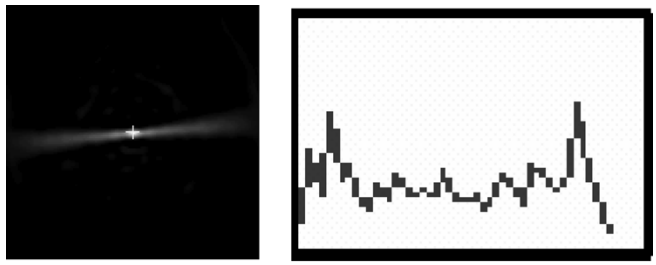

Fig. 5. A line source (a) was generated and its intensity profile (b) at the projection perpendicular to the line source was used for normalization.

Two different crystal lengths (5 and 10 mm) were modeled and compared with each other. A cylindrical PET with a diameter of 40 mm and a length of 5(10) mm was segmented into 58 discrete elements. This number of segments is slightly larger than the 52 elements in the 2-block experimental geometry described above because a depth of interaction of half the crystal depth was used which increased the effective radius. This was necessary because the curvature of the scanner cannot be neglected when the full FOV is simulated. Several point sources with different positions within the FOV were generated. The positions of the point sources were shifted from the center of the tomograph toward the edge of the FOV. The interaction position of the annihilation photons within each crystal segment was assigned to its center point at the depth of half the crystal thickness. The identification of the interacting crystal mimics the experimental conditions where due to the one-to one coupling between each crystal and an APD pixel, the crystal with the highest energy deposition is identified as the interacting crystal. The resultant coincident events were binned into 33 (radial) $\times$ 29 (angular) interleaved sinograms which are similar to the experimental sinograms except for the increased number of radial bins required to cover a $\sim$36 mm diameter FOV and the fact that azimuthal mashing is not used because it would cause angular undersampling due to the larger FOV. The sinograms were normalized before reconstruction.

The normalization was done by using a thin line source [Fig. 5(a)] taking the projection perpendicular to the line source and using the intensity profile [Fig. 5(b)] to correct the response along the line. The line source was placed on a transaxial tomograph plane and scanned. Only transaxial LORs were used for sinogram binning. The projection of this line from an observation view perpendicular to the line is expected to be an intensity profile with a square shape, if the normalization procedure is applied correctly. The intensity profile before the normalization correction (Fig. 5) shows less detected events toward the center of the tomograph. Since the intrinsic detector block sensitivity among the 12 detector blocks in the simulation is equal, this effect is caused mainly by the different crystal thickness for photons when penetrating an arched tomograph. This intensity profile thus reflects the relative efficiency of each LOR in the projection and its inverse can be used to normalize sinograms for these effects. In the simulation, the normalization vector that is determined from one of the projections can be applied for all other projections due to the assumption of identical intrinsic detector efficiencies.

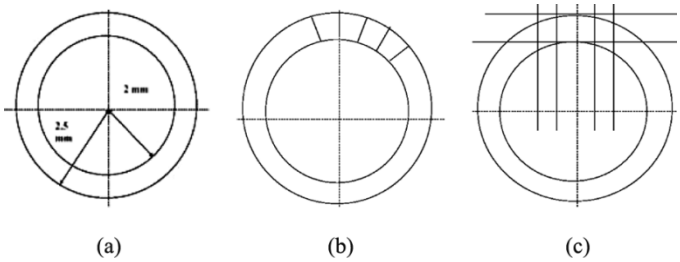

Fig. 6. Simulation geometries. (a) Cylindrical PET. (b) Discretized PET with no gaps. (c) Discretized PET with gaps between blocks (block detector geometry).

After reconstruction, the FWHM of each point source was measured and plotted as a function of its distance from the center of the tomograph.

The second version of the discretization was developed later and took the realistic gaps between the detector blocks into account. This version is a closer approximation to the RatCAP design and it will be used to model the probability matrix of RatCAP for ML-EM [7] image reconstruction. This discretization code places a grid of rectangular crystals organized in evenly spaced blocks over the original SimSET's cylindrical detector, rejecting events which do not fall within the blocks (Fig. 6).

RatCAP's geometry leads to incomplete sampling of the experimental data that result in zero efficiency bins (ZEBs). None of the modified SimSET versions could be used to efficiently model the characteristic RatCAP patterns. The first discretization method [Fig. 6(b)] ignores the gaps entirely. Although the second method [Fig. 6(c)] models the gaps and re-bins the events in a way that the sinograms have no ZEBs, they need to be arc corrected before reconstructing with filtered backprojection. Here we just used the unmodified cylindrical PET mode to create several activity objects with diameters between 1 and 4 mm, placed in different positions inside a field of view of about 36 mm. The resulting sinogram was multiplied by a pattern sinogram to create a realistic RatCAP sinogram with expected zero efficiency bins [Fig. 10(b)]. We performed a nearest neighbor 1-D interpolation in the radial direction to compensate the effect of the gaps. The interpolated image [Fig. 10(c)] was then compared to the ideal cylindrical PET with no gaps [Fig. 10(a)]. The simulated acquisition was taken in 2-D mode and the images were reconstructed by using a 2-D filtered backprojection.

The 7×13 sinograms obtained from the experimental data do not exactly mimic the real RatCAP data. As mentioned, the experimental setup consists of (only) two detector blocks and a phantom that is placed between them. To date, only the phantom can rotate and its rotation provides tomographic data. Since only coincident events between two opposing detector blocks have been taken into account, this experiment represents a tomograph with identical detector blocks and ring diameter as the RatCAP and a slightly different geometry in terms of the number of detector blocks, their position and the resulting coincidence lines. Although the experimental data do not represent the realistic RatCAP in some ways such as the number of detector blocks, size of the FOV and detector gaps, currently, it is the only method we have to test the detector blocks, electronics and

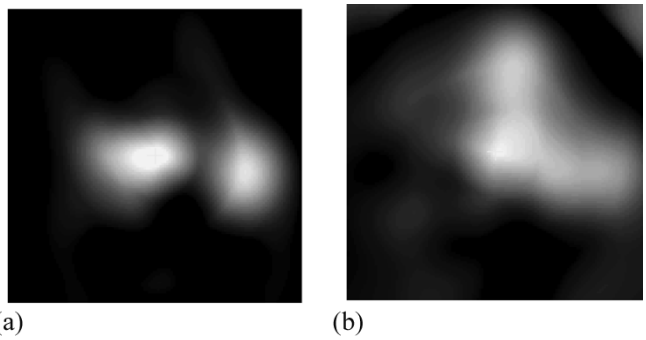

Fig. 7. Image of two rod sources (a) and an L-shaped source (b). Images were not normalized for detector efficiency variations.

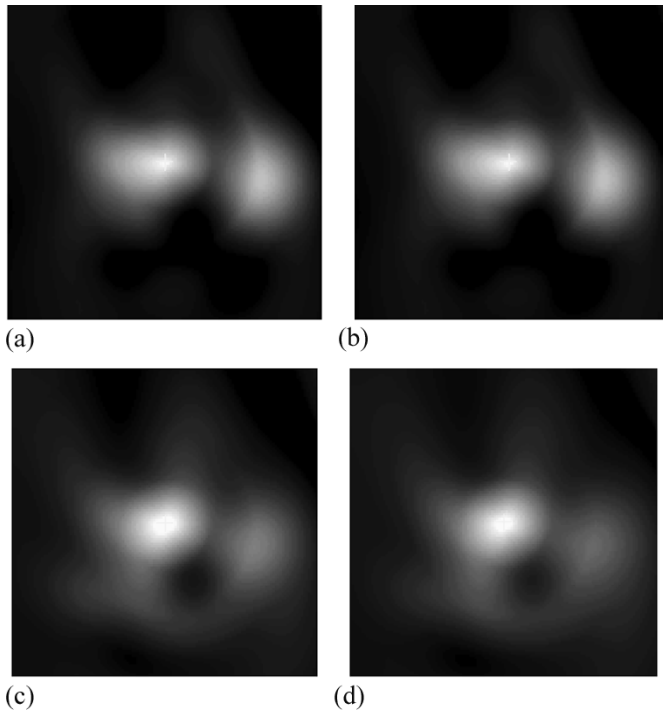

Fig. 8. Image of two point sources. (a) 2-D data mode. (b) 3-D mode with ring difference $= 1$. (c) 3-D mode with ring difference $= 3$. (d) 3-D mode with ring difference $= 5$.

DAQ system. Since the simulated data were not limited by the experimental conditions, the Monte Carlo modeling of RatCAP took almost all the physical details of the tomograph into account. Therefore, the simulated data were binned into sinograms that corresponded to a larger field of view and larger number of LORs.

III. Experimental Results

The first images of the two rod sources and the L-shaped source acquired on the rotational platform are illustrated in Fig. 7(a)–(b) and Fig.8(a)–(d). For the 2-D images (Fig. 7) only the axially direct lines of response that corresponded to the ring difference of zero were binned into (7×13) sinograms, and reconstructed with 2-D filtered back projection method. The point sources were 5 mm apart from each other and can be easily resolved in the image. From the left rod source, which was placed about 2 mm away from the center of the tomograph

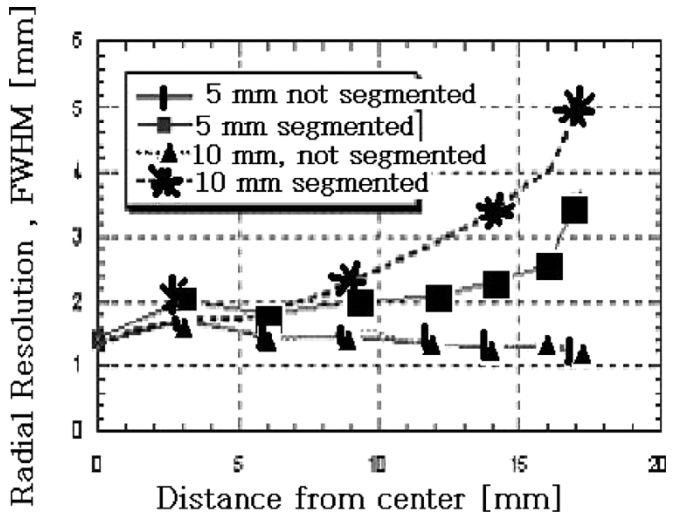

Fig. 9. PSF of a point source as a function of its distance from the center of the FOV for 4 different detector configurations: 1) RatCAP (40 mm ID) and 5 mm LSO crystal length (■), 2) RatCAP (40 mm ID) and 10 mm LSO crystal length (∗), 3) tomogarph with depth measurement capability (40 mm ID) and 5 mm LSO crystal length +), and 4) with depth measurement capability (40 mm ID) and 10 mm LSO crystal length (▲).

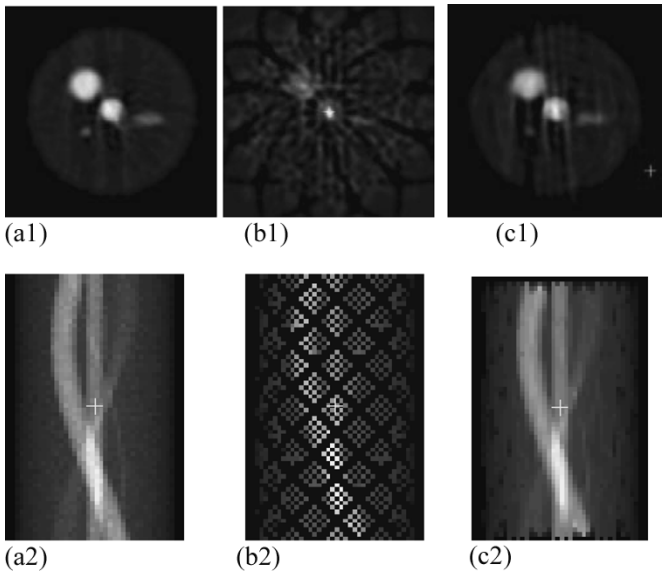

Fig. 10. (a1) Reconstructed image from a fully sampled sinogram (a2). (b1) Reconstructed image from a realistic RatCAP geometry sinogram (b2). (c1) Reconstructed image from interpolated sinogram (c2).

on a transaxial plane and near the axial center, the radial and tangential profiles were fitted with Gaussian functions and the average point spread function (PSF) was 2.2 ± 0.2 mm which includes the diameter of the source (0.5 mm). This is not the best spatial resolution achievable with the given experimental conditions. A more accurate measurement of the PSF of a single point source closer to the center has been reported in [3]. For the 2-D acquisition. the lack of septa was compensated by setting an energy threshold at 420 keV to reduce the scattered coincident events.

For the 3-D data, the oblique LORs were also added into the sinogram binning code which binned them into 64 sinograms (8 direct and 56 oblique sinograms). The sinograms were Fourier rebinned and reconstructed plane by plane with 2-D filtered backprojection. For the 3-D mode, we distinguished four different cases. In each case the maximum ring difference included in the reconstruction was set differently (from 0 to 5). These results are shown in Fig. 8(a)–(d).

IV. Simulation Results

The effect of the crystal length on the radial elongation is shown in Fig. 9. The data points of the lower curve are the radial resolutions of a simulated point source as a function of its distance from the center of an ideal (simulated) RatCAP tomograph where the exact interaction positions of the coincident events were used to bin the LORs into sinograms [nonsegmented as in Fig. 6(a)]. Clearly, changes in the crystal thickness (5 mm versus 10 mm) do not affect the radial resolution as expected. The square data points are the radial resolutions of a real (simulated) RatCAP with 5 mm crystal thickness that is incapable of determining the interaction positions of the annihilation gammas within the crystal [segmented as in Fig. 6(c)]. The radial resolution starts deteriorating at a distance of 12 mm from the center of the FOV. This radial elongation effect is even more significant when, in the same tomograph the crystal thickness increases from 5 to 10 mm (upper curve with star data points).

Another characteristic of RatCAP is the presence of the unnormalizable zero efficiency bins which will cause artifacts when the images are reconstructed using filtered backprojection. We modeled this effect with SimSET. In Fig. 10(b1) an ideal sinogram of a complete cylindrical modification of RatCAP has been generated and multiplied Fig. 10(b2) by a RatCAP efficiency sinogram with the typical patterns that result from the presence of the detector gaps. Using a simple one dimensional linear interpolation in the radial direction, we could estimate the value of the empty bins and recover the original sinogram by approximate means. Fig. 10(a1)–(c1) are the corresponding reconstructed images (filtered backprojection) of these sinograms.

V. Conclusion

A direct comparison has been made between Monte Carlo simulations of the RatCAP scanner and the experimental results obtained using a two-block LSO-APD detector rotational platform. These preliminary results were meant to test the experimental performance of the LSO+APD block detectors, and prove the ability of RatCAP to provide acceptable image quality applied with filtered backprojection. Due to the experimental conditions, no quantitative corrections were applied prior to the PSF measurements. In comparable small animal imaging systems such as the microPET R4, the typical corrections are detector normalization, arc, random, attenuation, and scatter corrections.

There were no septa incorporated in 2-D mode. The lack of septa was compensated for by setting an energy threshold at 420 keV to reduce scattered events. This seems to be compatible with Fourier rebinned 3-D data as long as the ring difference of the oblique LORs does not exceed five rings, which corresponds to an axial aperture of about 20 degrees.

Our group is currently working on the improvement of the energy resolution of the LSO-APD [8] and on reconstruction techniques such as ML-EM [7]. Many expected effects such as the presence of artifacts were evaluated by using a modified SimSET that is capable of representing a block detector tomograph. We came to the conclusion that by incorporating 5-mm crystals we can maintain a relatively constant radial resolution up to 12 mm away from the center of the tomograph (Fig. 9). This radius is large enough to cover the entire region of the rat's brain [3]. The reduction of the crystal length is a simple alternative to the placement of additional photo sensors to determine the depth of interaction information. The latter approach would be technically difficult with the dimensions of the RatCAP. Our simulation results show that the resolution can be improved from 2.3 to 1.8 mm at a distance from the center of 9 mm by using a 5-mm-long crystal instead of a 10-mm crystal. This improvement in resolution comes at cost of an approximate factor of 4 in coincidence sensitivity (no data shown). The selection of 5-mm crystals has another effect on the tomograph performance in terms of its energy resolution. This result was reported by Kriplani *et al.* [8] where the measured energy resolution of 5-mm detector arrays was significantly improved when compared to 10-mm crystals.

ACKNOWLEDGMENT

The authors sincerely acknowledge Proteus and CTI, Inc.

REFERENCES

[1] K. S. Hendrich, P. M. Kochanek, J. A. Melick, J. K. Schiding, K. D. Statler, D. S. Williams, D. W. Marion, and C. Ho, "Cerebral perfusion during anesthesia with fentanyl, isofluorane or pentobarbital in normal rats studies with arterial spin-labeled MRI," *Magn. Reson. Med.*, vol. 46, pp. 202–206, 2001.

[2] P. Vaska, D. J. Schlyer, C. L. Woody, S. P. Stoll, V. Radeka, and N. Volkow, "Imaging the unanesthetized rat brain with PET: a feasibility study," in *2001 IEEE Nucl. Sci. Symp. Medical Imaging Conf.*, vol. 3, 2001, pp. 1569–1571.

[3] P. Vaska, C. L. Woody, D. J. Schlyer, S. Shokouhi, S. P. Stoll, J. F. Pratte, P. O'Connor, S. Rescia, B. Yu, A. Villanueva Jr., A. Kriplani, A. Prakash, V. Radeka, and N. Volkow, "RatCAP: miniaturized head-mounted PET for conscious rodent brain imaging," *IEEE Trans. Nucl. Sci.*, vol. 51, pp. 2718–2722, 2004.

[4] W. W. Moses, P. R. G. Virador, S. E. Derenzo, R. H. Huesman, and T. F. Budinger, "Design of a high-resolution, high-sensitivity PET camera for human brains and small animals," *IEEE Trans. Nucl. Sci.*, vol. 44, no. 4, August 1997.

[5] M. Defrise, P. E. Kinahan, D. W. Townsend, C. Michel, M. Sibomana, and D. F. Newport, "Exact and approximate rebinning algorithms for 3-D PET data," *IEEE Trans. Med. Imaging*, vol. 16, no. 2, pp. 145–158, Apr. 1997.

[6] T. K. Lewellen, R. L. Harrison, and S. Vannoy, "The SimSET program," in *Monte Carlo Calculations in Nuclear Medicine, Medical Science Series*, M. Liungberg, S. E. Strand, and M. A. King, Eds. Bristol, U.K.: Inst. Phys., 1998, pp. 77–92.

[7] L. A. Shepp and Y. Vardi, "Maximum likelihood reconstruction in emission tomography," *IEEE Trans. Med. Imag.*, vol. MI-1, pp. 113–122, 1982.

[8] A. Kriplani, S. P. Stoll, S. Shokouhi, D. J. Schlyer, A. Villanueva Jr., P. Vaska, and C. L. Woody, "Comparison of experimentally measured light output with Monte Carlo simulations from LSO crystals," in *IEEE Medical Imaging Conf.*, Oct. 19–26, 2003.

[9] P. Vaska, S. P. Stoll, C. L. Woody, D. J. Schlyer, and S. Shokouhi, "Effects of inter-crystal cross-talk on multi-element LSO/APD PET detectors," *IEEE Trans. Nucl. Sci.*, vol. 50, pp. 362–366, 2003.